∷ cogent
engineering

CIVIL ENGINEERING | RESEARCH ARTICLE

Evaluation of seismic displacement demand for unreinforced masonry shear walls

Jayaprakash Vemuri[1]*, Syed Ehteshamuddin[1] and Subramaniam V. L. Kolluru[1]

*Corresponding author: Jayaprakash Vemuri, Department of Civil Engineering, IIT Hyderabad, Sangareddy, Telangana 502285, India
E-mail: ce13p1006@iith.ac.in

Abstract: Unreinforced, non-engineered low-strength brick masonry structures comprise a large percentage of buildings in the Himalayan region and have been extensively damaged in recent earthquakes. Due to the high seismic hazard of the region and the inherent vulnerability of non-engineered masonry structures, a seismic assessment of masonry construction in this region is imperative. In this study, a suite of strong ground motions is developed using data from major Himalayan earthquakes. Using a mechanistic-based procedure for predicting the monotonic load envelope which identifies limit states of cracking, strength, and collapse using stress-based criteria, a hysteretic model was calibrated to experimental data of unreinforced masonry shear walls. Nonlinear time history analyses are performed on the validated single degree of freedom models of two unreinforced masonry walls. The analytical results correlate well with observed damage to masonry structures in Himalayan earthquakes. Peak ground acceleration of ground motion is observed to be the key parameter influencing displacement of walls. A linearly increasing trend is observed between the PGA and the observed displacement up to a PGA value of 0.1g. A weak correlation is observed between displacement and ground motion frequency parameters.

Subjects: Seismology; Structural Engineering; Georisk & Hazards

ABOUT THE AUTHORS

Jaya Prakash Vemuri is a graduate student at the Indian Institute of Technology Hyderabad. His research interests include characterization of ground motions, generation of synthetic ground motions and nonlinear time history analyses of structures.

Syed Ehteshamuddin is a graduate student at the Indian Institute of Technology Hyderabad. His research interests include structural dynamics, mechanics of masonry, seismic assessment of masonry structures and low-cost construction materials.

Kolluru Subramaniam is a professor at the Indian Institute of Technology Hyderabad. He holds a Ph.D. from Northwestern University. His research interests include behavior of concrete and masonry structures, structural strengthening and FRP based repair of structures and blast analysis and mitigation.

PUBLIC INTEREST STATEMENT

The Himalayan region has high seismic hazard and has witnessed several destructive earthquakes in the past. Unreinforced masonry (URM) structures comprise the bulk of structures prevalent in this region. Recent Himalayan earthquakes have caused extensive damage to URM structures. To understand the severe damage to URM structures, nonlinear time history analysis is essential. In this study, a suite of strong ground motions from major Himalayan earthquakes is developed. Two URM walls based on the similarity of their material and geometric properties with URM walls in the Himalayan region were selected. The hysteric behavior of both walls was validated with observed experimental behavior using a cyclic model. Results from the analyses correlate well with actual damage to masonry structures recorded in post-earthquake studies conducted in the region. The study also determines the influence of the different ground motion parameters on the displacement of the URM wall.

∷ cogent · oa

✦ cogent ·· engineering

1. Introduction

The Alpine-Himalayan region which covers the entire Himalayan range of India is the second most active seismic belt in the world (Sinvhal, 2010). Some recent earthquakes which have occurred in this region include: 1991 Uttarkashi [M 6.8], 1999 Chamoli [M 6.8], 2005 Kashmir [M 7.6], 2011 Sikkim [M 6.9], 2015 Nepal [M 7.8]. A large percentage of the building stock in the Himalayan region consists of unreinforced brick masonry (URM) structures, unreinforced adobe or block masonry structures and stone masonry structures. The poor performance of stone masonry walls in the Himalayan belt has been reported (Ali et al., 2013) and experimental and analytical studies on stone masonry walls are also available (Ahmad, Ali, Ashraf, Alam, & Naeem, 2012). The percentage of building stock that is composed of brick masonry, unreinforced adobe and block masonry construction in India, obtained from Prompt Assessment of Global Earthquakes for Response (PAGER) survey is 69% for Unreinforced Fired Brick masonry (PAGER database, 2007). Unreinforced brick masonry structures are also widely prevalent in the Himalayan region of Pakistan (Bothara & Hicyilmaz, 2008) and it has been reported that these structures were "non-engineered" and proportioned to sustain only gravity loads (Javed, Naeem, & Magenes, 2008; Naseer, Naeem, Hussain, & Ali, 2010). There are two types of residential structures prevalent in the region: *Katcha* (non-permanent) and *Pucca* (permanent). The *Katcha* house has mud and stone rubble walls with cement-sand mortar with a mud roof supported on timber beams to support heavy mud insulation and snow load. The *Pucca* house has usually stone rubble or fired brick walls and the load-bearing unreinforced masonry (URM) walls support a heavy reinforced concrete slab on top (Durrani, Elnashai, Hashash, Kim, & Masud, 2005). Recent earthquakes have exposed the seismic vulnerability of URM structures, which have been either severely damaged or have completely collapsed (Durrani et al., 2005; Rai et al., 2012; Whitney & Agrawal, 2017). Traditional clay brick masonry structures performed poorly, and shear failure of brick walls was noticed with diagonal cracks. Due to the high seismic hazard of the Himalayan region and the inherent vulnerability of low strength masonry structures, a seismic evaluation of masonry construction is imperative.

Evaluation of seismic vulnerability of URM buildings requires a methodology for assessing the performance of such structures subjected to horizontal forces generated by earthquake ground motion. Simplified techniques for seismic assessment of specific URM buildings have been presented in several case studies (Formisano, 2012; Formisano, Florio, Landolfo, & Mazzolani, 2011; Formisano & Marzo, 2017). Seismic fragility functions for masonry buildings have been developed using the displacement based earthquake loss assessment method (Ahmad & Ali, 2017; Ahmad, Ali, Crowley, & Pinho, 2014; Ahmad, Crowley, Pinho, & Ali, 2010a; Ahmad, Crowley, Pinho, & Ali, 2010b). Ahmad et al. (2011) developed a fast building seismic screening method (FBSS) for masonry structures to assess their expected level of performance at a given site. The study used a site-specific and structure-specific methodology to develop simplified graphical methods, which can be used to predict the damage level of a system for a given seismic demand. Other literature on masonry is focussed either on the out-of-plane behavior of unreinforced masonry or reinforced masonry walls. Shear failure of unreinforced brick masonry walls, which has been predominantly observed in the Himalayan rural dwellings (Shrikhande Rai, Narayan, & Das, 2000) and elsewhere (Moore, Kobzeff, Diri, & Arnold, 1988; Moon et al., 2014; Reitherman, 1985; Somers et al., 1996) is an under-investigated area. A large number of URM shear walls tested in laboratories are subjected to static monotonically applied loads, which are more representative of wind loads than earthquake loadings (Boussabah & Bruneau, 1992). Under seismic excitation, masonry exhibits significant inelastic displacement associated with cracking and its hysteretic behavior is characterized by strength and stiffness degradation. The post-cracking dynamic behavior of URM walls under seismically induced in-plane shear forces can be understood by subjecting URM walls to cyclic loads. Limited experimental studies are available on shear behavior of unreinforced clay brick walls (Abrams, 1992; Ali et al., 2012; Alsuwwi, Hassan, Awwad, & Ahmad, 2015; Anthoine, Magonette, & Magenes, 1995; FEMA 307, 1999; Khan et al., 2013; Magenes & Calvi, 1992). Available

experimental results, both cyclic and monotonic, for URM walls, vary widely due to variation in test materials, the geometry of tested walls and experimental boundary conditions which may not be similar to actual boundary conditions (Bosiljkov, Page, Bokan-Bosiljkov, & zarnić, 2010; FEMA 307, 1999). Thus the expected performance of URM structures under anticipated earthquakes remains uncertain and inconclusive. There is lack of data to bridge the gap towards the performance-based design of unreinforced masonry structures (Bosiljkov et al., 2010).

To bridge this gap, the displacement demand on URM structures may be evaluated analytically. However, the seismic response of URM walls is affected by the complex interaction of mortar and brick and the interface at the joints due to layering patterns. There is a lack of experimentally validated hysteretic models to explain the complex cyclic behavior of URM walls. This challenge to nonlinear time history analyses can be overcome by adopting a mechanistic-based approach to derive the monotonic load envelope for identifying various limit states of cracking, strength, and collapse using stress-based criteria. A hysteretic model may then be calibrated to available experimental test results and then be used to analyse an analytical model of a URM wall under seismic ground motions.

In the past, the lack of seismographs in the Himalayan region, combined with the absence of data sharing mechanism across government organizations, contributed to a poor understanding of the actual uncertainty due to ground motion in the Himalayas. As uncertainty in ground motion strongly depends on the local site conditions and geological profile of the area, for an accurate seismic assessment of URM walls it is essential to characterize the local ground motions recorded in the Himalayan region. Ground motion characteristics such as peak ground acceleration and frequency content are vital contributors to structural response. Correlation studies between damage indices for reinforced concrete buildings and seismic acceleration parameters have been performed (Elenas, 2001). However, such a study is unavailable for URM structures. A proper evaluation of Himalayan ground motion characteristics and their relationship with displacements will identify the critical parameters. The identified parameters may contribute towards proper design and rehabilitation of URM structures.

In this paper, seismic displacement demand on low-strength URM shear walls subjected to ground motions from the Himalayan region is evaluated. Two URM walls based on the similarity of their material and geometric properties with URM walls in the Himalayan region (Bureau of Indian Standards, 1991) were selected. The monotonic capacity curve is generated using a mechanistic-based procedure, which identifies limit states of cracking, strength, and collapse using stress-based criteria. The hysteretic behavior of both walls was validated with observed quasi-static experimental behavior using a Pivot model. The parameters of the Pivot model are calibrated for both walls using least squares optimization, and a good match is obtained between experimental and analytical hysteresis curves. The suite of strong ground motions for nonlinear time history analyses is developed using data obtained from major Himalayan earthquakes, which cover different regions of the Himalayan arc and hence are representative of the seismic hazard of the region. The influence of the different ground motion parameters on the level of damage is determined.

2. Cyclic load response of shear walls

Under cyclic loads, a URM wall may fail by three mechanisms: rocking, shear or sliding. Out of these three modes, shear failures are predominant in walls with aspect ratios (height/length) less than 2.0. Many existing URM walls in the Himalayan region fall below this aspect ratio and are dominated by diagonal in-plane cracking. The URM walls are usually weak and support a heavy slab on top (Shrikhande et al., 2000). The compressive strength of bricks in the Himalayan region (Uttar Pradesh) lies in the range of 10–20 MPa and the compressive strength of mortar lies in the range of 3 to 5 MPa (Bureau of Indian Standards, 1991). Shear failures of URM walls, for the range of compressive strengths typical in such construction, have distinct features as shown in Figures 1 and 2. Mild hysteresis characterizes pre-cracking behavior. The walls initially crack in flexure

cogent ·· engineering

Figure 1. (a) Failure of masonry wall; (b) stress block of Masonry wall; (c) backbone curve of masonry wall.
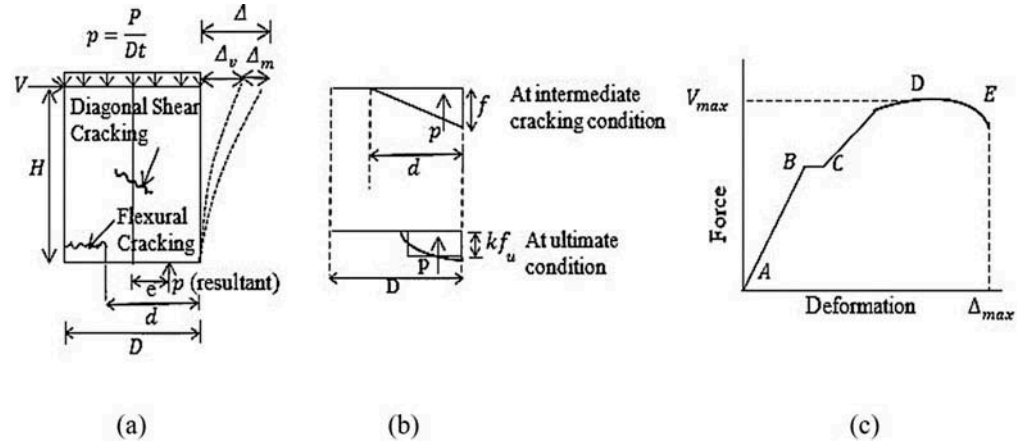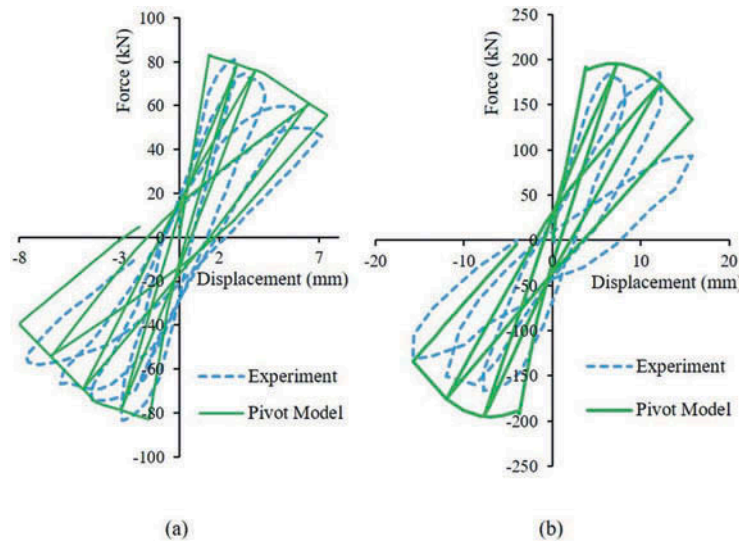

Figure 2. Envelope curve and hysteresis behavior of shear walls: (a) Masonry wall with failure mode of diagonal shear cracking through mortar joints (stepped cracking); (b) Masonry wall with the failure mode of shear-tensile cracking of bricks.

followed by diagonal cracking which occurs close to the peak shear force (Magenes & Calvi, 1992). Strength degradation takes place after the onset of visible diagonal cracking which is associated with the attainment of the peak lateral force. Post-peak response is characterized by rapid strength and stiffness degradation and also higher energy dissipation. Failure occurs by diagonal shear cracking through mortar joints. The ultimate displacement in shear failure is lower as compared with other common failure modes of URM walls. Walls with higher axial stress exhibit similar response to that of wall failing in shear, but had greater strength due to higher axial stress which increases the resistance in shear.

The monotonic shear-deformation ($V - \Delta$) response of the wall under constant applied vertical stress forms the backbone to the cyclic load response. An incremental procedure for obtaining the deformation considering the different damage mechanisms was used for obtaining the envelope curve (Penelis, 2006). In the analysis, the load deformation curve ($V - \Delta$ curve) is generated at each increment of lateral force, by combining deformations due to flexure and shear, while checking the modes of failure by comparing lateral force with the shear and flexural strengths. The flexural deformation, Δ_m is calculated by generating the curvature diagram at each increment of lateral force using equilibrium and deformation compatibility conditions on the section. The compressive stress is assumed to be linear with strains. Tensile strength of masonry is neglected. Moment of Inertia is revised at each increment of the lateral load based on the effective uncracked

section. The curvature diagram is then integrated to get the deformation due to flexure. This formulation is slightly conservative. The shear component Δ_v is calculated as a bilinear curve, which is governed by elastic shear modulus in the pre-cracking regime and effective shear modulus in the post-cracking regime. Effective shear modulus is taken equal to 90 times of masonry compressive strength which was established from statistical analyses of experimental results (Penelis, 2006). Shear response is a bilinear curve which is marked by diagonal cracking of shear walls followed by a softening effect due to a reduction in the effective shear area and is modelled as a parabolic fit. In the backbone curve as shown in Figure 1, A is the origin and B denotes the point of initiation of a flexural crack. After cracking in flexure, an unreinforced wall resists moment through the force couple that is generated as the resultant of vertical compressive stress shifts towards the wall toe as the total vertical force was kept constant. This shift in the resultant compressive stress of constant magnitude resulted in a decrease in lateral stiffness but did not reduce the overall shear strength and is represented by line CD. Point D signifies peak response of wall. The final portion DE is marked by both strength and stiffness degradation due to a reduction in the effective shear area.

Flexural strength is given by (Magenes & Calvi, 1997):

$$V_r = \frac{pDt}{2\alpha_v}\left(1 - \frac{p}{kf_u}\right) \tag{1}$$

where P is the axial load, $p = P/Ht$ is the axial stress, H is the wall height, D is the length of the wall, t is the thickness of the wall, f_u is the masonry compressive strength, k is a coefficient which accounts for vertical stress distribution at the compressed toe, $\alpha_v = M/(VD)$ is the shear ratio.

Shear strength is given by (Magenes & Calvi, 1997):

$$V_d = Dt\tau_u; \ \tau_u = \text{minimum } (\tau_{cs}; \tau_{ws}; \tau_b) \tag{2}$$

τ_{cs} refers to shear stress relevant to the cracked section and is given as:

$$\tau_{cs} = \frac{1.5c + \mu p}{1 + \frac{3c\alpha_v}{p}} \tag{3}$$

τ_{ws} refers to shear stress of the whole section and is given as:

$$\tau_{ws} = \frac{c + \mu p}{1 + \alpha_v} \tag{4}$$

τ_b refers to shear stress based on cracking of bricks and is given as:

$$\tau_b = \frac{f_{bt}}{2.3}\sqrt{1 + \frac{p}{f_{bt}}} \tag{5}$$

where c is the cohesion of joint, μ is the coefficient of friction of joint, f_{bt} is the tensile strength of brick. The role of weak head joints and a correction of the friction and cohesion coefficient which is given by $c' = kc$ and $\mu' = k\mu$ (Mann & Muller, 1982)

$$k = \frac{1}{1 + \mu 2\frac{\Delta_y}{\Delta_x}} \tag{6}$$

where Δ_x and Δ_y are the length and height of brick unit respectively. Two shear walls with separate series of static tests are considered here to generate the backbone curve and to get the cyclic load response (Anthoine et al., 1995; Magenes & Calvi, 1992). The geometric and material properties are summarized in Table 1.

The multilinear-plastic pivot model available in SAP2000 (Computers and Structures Incorporated, 2012) was used to model the behavior of the URM wall. The link element enables

cogent ·· engineering

Table 1. Geometric and material properties for shear walls (Anthoine et al., 1995; Magenes & Calvi, 1992)		
Property	**Wall 1**	**Wall 2**
Height of Wall, H	1350 mm	3000 mm
Length of Wall, D	1000 mm	1500 mm
Thickness of Wall, t	250 mm	380 mm
Vertical Compressive Stress, p	0.6 MPa	1.24 MPa
Brick Compressive Strength, f_b	16 MPa	19.7 MPa
Brick Direct Tensile Strength, f_{bt}	1.22 MPa	1.07 MPa
Mortar Compressive Strength, f_m	3.31 MPa	4.33 MPa
Masonry Compressive Strength, f_u	6.2 MPa	7.9 MPa
Joint Cohesion, c	0.23 MPa	0.21 MPa
Corrected Joint Cohesion, c'	0.17 MPa	0.14 MPa
Joint Coefficient of Friction, μ	0.58	0.81
Corrected Joint Coefficient of Friction, μ'	0.43	0.55

the user to replicate cyclic behavior of the URM wall, by defining four pivot parameters, α_1, α_2, β_1 and β_2 which control the shape of the hysteresis loop, strength degradation and stiffness degradation. The parameters of the pivot model were calibrated using the optimization technique of least squares method, with the objective of minimizing the error with respect to the experimental results. For the wall reported by Anthoine et al. (1995) the four pivot parameters, α_1, β_1, α_2 and β_2 were obtained as 0.90. The parameters are equal in magnitude because of symmetry of cyclic response and absence of pinching. Figure 2 shows the good match between the experimental hysteresis loops and the loops obtained from the pivot model. Another URM shear wall, reported by Magenes and Calvi (1992) had a higher imposed load. For this wall, the four pivot parameters, α_1, β_1, α_2 and β_2 were obtained to be equal to 0.90. Figure 2(b) shows the match between the experimental hysteresis loops and the loops obtained from the pivot model. The parameter values are similar for both walls, owing to the fact that both walls had a symmetric response without pinching. From Figure 2, displacement limit states corresponding to cracking, strength and collapse were identified as 0.5, 2 and 7.5 mm for wall 1 and 1, 3.5 and 16 mm for wall 2, respectively.

3. Strong motions and their characteristics

Seismic activity in the Himalayan region is primarily due to the collision of Indian and Eurasian plates (Ni & Barazangi, 1984; Seeber & Armbruster, 1981). In this region, the Indian plate subducts beneath the Eurasian plate, the consequent build-up of elastic strain energy causes the region to be highly seismically active. Major fault systems which span the length of the Himalayan arc are the Main Frontal Thrust (MFT), the Main Boundary Thrust (MBT), the Main Central Thrust (MCT) and the Indus Suture Thrust (Kayal, 2001). Many large (M > 7.0) and great earthquakes (M 8.0 and above) frequently occur between the MCT and MBT (Chopra, 2012). Bilham and Wallace (2005) predict that four large earthquakes may occur within the inferred seismic gap areas.

To understand the damage in recent Himalayan earthquakes to URM walls, a suite of strong ground motions is developed from unscaled, actual ground motions from major Himalayan earthquakes. Strong-motion data from the Main Himalayan Seismic Belt for Uttarkashi (1991), Chamoli (1999), Nepal (2015) and Sikkim (2011) earthquakes were acquired from Consortium of Organisations for Strong-Motion Observation Systems (Consortium of Organizations for Strong-Motion Observation Systems [COSMOS], 2015) and Program for Excellence in Strong Motion Studies (Program for Excellence in Strong Motion Studies [PESMOS], 2015). Two strong-motion records from the Kashmir (2005) earthquake obtained from the Mid-America Centre for Earthquake Engineering (Personal Communication, 2016) were also used in the analyses. These five earthquakes were selected to represent the seismic hazard of the region. These

high moment magnitudes earthquakes have their origins in the Himalayan region and represent the variation in local topography as they cover different regions of the Himalayan arc.

The 1991 Uttarkashi earthquake (M_w = 6.8) was associated with the MCT zone of the Himalaya (Mandal, Rastogi, & Gupta, 2000). The 1999 Chamoli earthquake (M_w = 6.8) also occurred along the sub-faults of the MCT (Jain et al., 1999). Both the 1991 Uttarkashi and the 1999 Chamoli were classified as "shallow". The epicentres for the two earthquakes were close to each other and had similar tectonic environment (Joshi, 2006). Strong ground motion recording stations for the two earthquakes were located in a range of 20km to 160km from the epicentres. The 1991 Uttarkashi earthquake triggered recordings at 13 stations, while the main shock of the 1999 Chamoli earthquake triggered 10 stations.

The 2011 Sikkim earthquake (M_w = 6.9) had a more complex origin (Rajendran, Rajendra, Thulasiraman, Andrews, & Sherpa, 2011) as typical earthquakes in this region are inter-plate in nature, however, the Sikkim earthquake seems to be triggered from an intraplate source on the Eurasian Plate. The Sikkim earthquake was also classified as "shallow" and triggered strong motion accelerographs at seven stations. The 2015 Nepal earthquake (M_w = 7.8) was located between the major thrusts MCT and MBT (Parameswaran et al., 2015). The 2005 Kashmir earthquake (M_w = 7.6) which caused widespread destruction to URM structures, also occurred along the off-shoots of the MBT (Mandal, Chadha, Kumar, Raju, & Satyamurty, 2007).

Figure 3(a)–(c) shows the pseudo-spectral acceleration (PSA) at 5% damping, for horizontal components of strong ground motions from the Uttarkashi (1991), the Chamoli (1999) and the Sikkim (2011) earthquakes. The response spectra for Zone IV from the Indian code of design practice, IS: 1893, which forms the basis of the design of structures in India is also shown in the figures for comparison. It may be observed that response spectra of 2011 Sikkim earthquake exceed the Zone 4 level of IS: 1893 and exhibit sharp peaks around 0.1 sec followed subsequently by a sharp drop. This indicates the presence of very high-frequency content in the ground motion. As compared to the Sikkim quake, response spectra from the Uttarkashi and the Chamoli earthquakes have a wide acceleration sensitive region. Figure 4 shows PSA (5% damping) for horizontal components of strong ground motions from the 2005 Kashmir (M_w = 7.6) and the 2011 Nepal (M_w = 7.8) Earthquakes. As compared to the Uttarkashi, Chamoli and, Sikkim earthquakes, the spectra from Nepal and Kashmir show very wide acceleration sensitive region. The response spectra for Zone V from IS 1893 is also shown for comparison: it is observed that response spectra exceed the Zone V level of the IS: 1893 prescribed level. Further, the response spectra have significant long-period components indicating the presence of significant low frequency content. The presence of low frequency

Figure 3. Response spectra of strong ground motions: a) 1991 Uttarkashi earthquake b) 1999 Chamoli earthquake c) 2011 Sikkim earthquake.
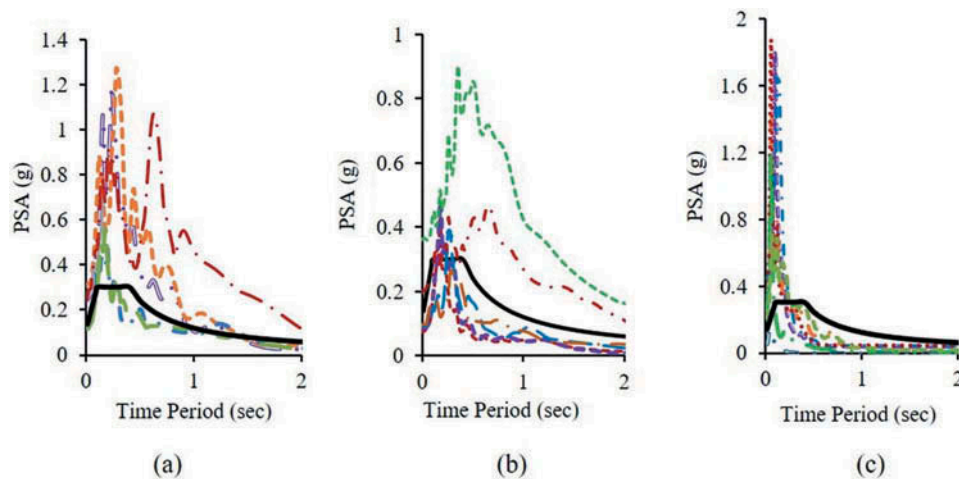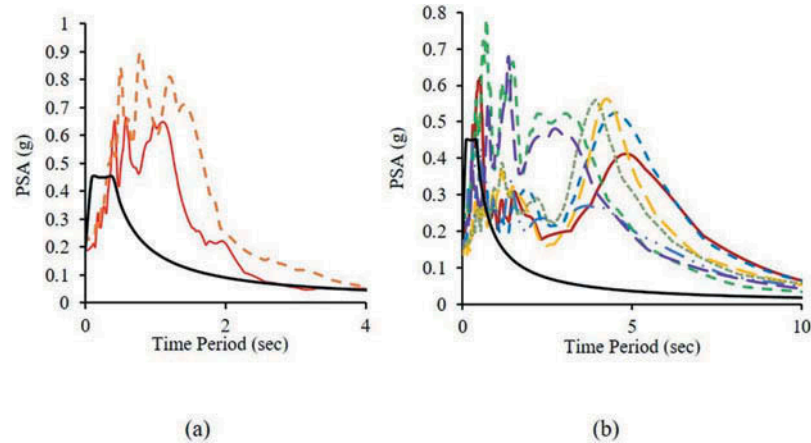
Figure 4. Response spectra of strong ground motions a) 2005 Kashmir earthquake b) 2015 Nepal earthquake.

(a)   (b)

content is also caused due to the locations of the recording stations: ground motions from Nepal were recorded in the Kathmandu valley and, four sites were classified as sedimentary and, one site was classified as rock. Typically, the estimation of frequency content in ground motions is typically done using Fast Fourier transforms (FFT), which transform a time history into a frequency domain and highlight the frequency ranges at which energy is concentrated. As the computation of FFTs is tedious, single parameter estimates, such as the predominant period, T_p and mean period, T_m are used in this study, to characterize the frequency content of ground motions used for NTHA.

Typical URM walls are very stiff and lie in the short period range. Essentially, the walls will be more prone to damage by high-frequency waves. Response spectra of ground motions considered in the present study show wide variation: while the Sikkim earthquake represents high-frequency ground motion recorded on rock sites, the Nepal earthquake represents ground motions with low-frequency content. All ground motions from the Nepal and Sikkim earthquakes exceed the code recommended response spectra. Frequency content in the ground motions from the Uttarkashi and the Chamoli earthquakes spans across low- to high-frequency range. Response spectra for the Uttarkashi and Chamoli earthquakes lie both below and above the code prescribed limits. Using the available variety of ground motions, the expected damage to URM walls analyzed in this study, having T_n = 0.1 sec and T_n = 0.3 sec, would provide for understanding the damage/fragility to the URM wall structural system within the range of structural parameters expected in the field.

4. Results from nonlinear time history analyses

NTHA is a rational and rigorous method for evaluating the seismic performance of a structure. In this study, NTHA was performed in SAP2000 using Nonlinear Direct Integration History method. The Hilbert-Hughes-Taylor algorithm ($\gamma = 0.5$, $\beta = 0.25$, $\alpha = 0$) was used with a step time of 0.02s. The mass-proportional and stiffness proportional coefficients for Rayleigh damping were computed using standard procedure (Chopra, 2012). Table 2 to 6 display results from NTHA performed on the two URM walls. Peak displacements of both URM walls are identified from the output time histories and are tabulated. The tables include the name of the recording station, soil type prevalent at the station and epicentral distance of the station. Frequency content in the ground motion is represented using single parameters, such as Mean Period, T_m and Predominant Period, T_p. The PGA, peak ground velocity (PGV), and the peak ground A/V ratio for ground motions are also tabulated. The site class is defined based on shear wave velocity, V_{s30} (Mittal, Kumar, & Ramhmachhuani, 2012). Class A corresponds to firm/hard rocks with values of V_{s30} between 700 m/s to 1620 m/s, class B corresponds to soft to firm rocks, with values of V_{s30} between 375 m/s to 700 m/s and class C corresponds to soil, with values of V_{s30} below 375 m/s.

cogent • engineering

S. No.	EQ record	Soil Type	Dist. (km)	PGA (g)	PGV (m/s)	A/V (g/m/s)	Frequency Parameter (s)		Drift Wall 1	Drift Wall 2
							T_p	T_m	U (mm)	U (mm)
1	Abbottabad-EW	A	60	0.24	0.42	5.50	0.78	0.99	7.58	16
2	Abbottabad-NS	A	60	0.19	0.29	6.32	0.58	0.86	7.58	16

Table 2. 2005 Kashmir earthquake: summary of results

cogent · engineering

Table 3. 2015 Nepal earthquake: summary of results

S. No.	EQ record	Soil Type	Dist. (km)	PGA (g)	PGV (m/s)	A/V (g/m/s)	Frequency Parameter (s)		Drift Wall 1 U (mm)	Drift Wall 2 U (mm)
							T_p	T_m		
1	Kirtipur-1	A	75.8	0.14	0.29	4.78	0.26	0.39	7.58	16
2	Kirtipur-2	A	75.8	0.28	0.30	9.17	0.26	0.47	7.58	16
3	Tribhuvan-1	C	77.1	0.24	0.91	2.60	1.37	1.82	7.58	16
4	Tribhuvan-2	C	77.1	0.21	0.76	2.74	0.7	1.69	7.58	16
5	Pulchowk-1	C	79.3	0.22	0.68	3.09	0.44	1.17	7.58	16
6	Pulchowk-2	C	79.3	0.13	0.71	1.86	1.38	1.45	7.58	16
7	Sanothimi-1	C	83.7	0.17	0.76	2.19	3.48	2.82	7.58	16
8	Sanothimi-2	C	83.7	0.14	0.77	1.83	1.16	2.15	7.58	16
9	Kantipath-1	A	59.9	0.16	1.07	1.48	3.48	1.71	7.58	16
10	Kantipath-2	A	59.9	0.19	0.98	1.92	0.52	1.19	7.58	16

Table 4. 1999 Chamoli earthquake: summary of results

S. No.	EQ record	Soil Type	Dist. (km)	PGA (g)	PGV (m/s)	A/V (g/m/s)	Frequency Parameter (s)		Drift Wall 1	Drift Wall 2
							T_p	T_m	U (mm)	U (mm)
1	Almora-L	A	106	0.03	0.02	1.14	0.24	0.35	2.7	2.35
2	Almora-T	A	106	0.03	0.02	1.47	0.26	0.36	1.9	1.57
3	Barkot-L	A	118	0.02	0.01	1.83	0.18	0.26	0.82	0.82
4	Barkot-T	A	118	0.02	0.01	2.08	0.22	0.25	3.89	1.06
5	Chinaylisaur-L	A	103	0.05	0.03	1.35	0.32	0.37	2.2	2.34
6	Chinaylisaur-T	A	103	0.05	0.03	1.66	0.3	0.40	2.7	2.59
7	Ghansiali-L	A	73	0.08	0.04	2.05	0.18	0.24	4	3.93
8	Ghansiali-T	A	73	0.07	0.03	2.20	0.18	0.24	4	4.86
9	Gopeshwar-L	A	14	0.20	0.23	0.87	0.66	0.79	7.58	16
10	Gopeshwar-T	A	14	0.36	0.45	0.79	0.36	0.67	7.58	16
11	Joshimath-L	A	17	0.06	0.09	0.71	0.16	0.41	4	4.55
12	Joshimath-T	A	17	0.07	0.03	2.23	0.24	0.78	7.58	13.62
13	Lansdowne-L	A	102	0.01	0.002	3.07	0.08	0.93	0.16	0.146
14	Lansdowne-T	A	102	0.01	0.02	0.31	0.1	0.20	0.17	0.149
15	Tehri-L	A	88	0.05	0.05	1.19	0.3	0.42	4	3.81
16	Tehri-T	A	88	0.06	0.05	1.16	0.44	0.47	5.3	5.73
17	Ukhimath-L	A	29	0.10	0.06	1.77	0.28	0.42	7.58	9.07
18	Ukhimath-T	A	29	0.10	0.07	1.33	0.28	0.37	7.58	8.36
19	Uttarakashi-L	A	94	0.06	0.05	1.36	0.2	0.37	3.8	4.25
20	Uttarakashi-T	A	94	0.05	0.04	1.50	0.4	0.33	7.58	11.64
21	Roorkee-L	C	162	0.06	0.03	1.70	1.5	1.8	7.58	16
22	Roorkee-T	C	162	0.05	0.04	1.09	1.3	1.8	7.58	16

Table 5. 2011 Sikkim earthquake: summary of results

S. No.	EQ record	Soil Type	Dist. (km)	PGA (g)	PGV (m/s)	A/V (g/m/s)	Frequency Parameter		Drift Wall 1	Drift Wall 2
							T_p	T_m	U (mm)	U (mm)
1	Gezing—H1	A	16	0.45	0.93	0.48	0.12	0.12	7.58	16
2	Gezing—H2	A	16	0.34	2.39	0.14	0.06	0.16	7.58	16
3	Mangan-H1	A	52	0.39	0.98	0.40	0.06	0.09	7.58	16
4	Mangan-H2	A	52	0.27	0.41	0.66	0.08	0.11	7.58	16
5	Gangtok-H1	A	51	0.26	0.19	0.82	0.06	0.11	7.58	16
6	Gangtok-H2	A	51	0.29	0.36	1.42	0.06	0.14	7.58	16
7	Chungthang-H1	A	66	0.36	0.77	0.47	0.10	0.12	7.58	16
8	Chungthang-H2	A	66	0.24	0.68	0.35	0.10	0.12	7.58	16
9	Singtam-H1	A	28	0.22	0.35	0.63	0.06	0.16	7.58	16
10	Singtam-H2	A	28	0.09	0.07	1.29	0.08	0.14	2	2
11	Melli-H1	A	78	0.26	0.09	2.81	0.06	0.07	3.3	3.3
12	Melli-H2	A	78	0.27	1.56	0.17	0.06	0.11	7.58	16
13	Siliguri-H1	B	103	0.16	0.11	13.47	0.16	0.32	7.58	16
14	Siliguri-H2	B	103	0.20	0.10	20.71	0.20	0.29	7.58	16

cogent · engineering

Table 6. 1991 Uttarkashi earthquake: summary of results

| S. No. | EQ record | Soil Type | Dist. (km) | PGA (g) | PGV (m/s) | A/V (g/m/s) | Frequency Parameter | | Drift Wall 1 | Drift Wall 2 |
							T_p	T_m	U (mm)	U (mm)
1	Almora-L	A	158	0.02	0.01	1.33	0.26	0.39	1.4	1.69
2	Almora-T	A	158	0.02	0.01	1.7	0.22	0.40	1.58	1.29
3	Barkot-L	A	53	0.08	0.05	1.83	0.12	0.23	6.6	7.8
4	Barkot-T	A	53	0.10	0.06	1.64	0.26	0.25	4.4	5.17
5	Bhatwari-L	A	53	0.25	0.30	0.83	0.28	0.42	7.58	16
6	Bhatwari-T	A	53	0.25	0.18	1.41	0.62	0.54	7.58	16
7	Ghansiali-L	A	42	0.12	0.08	1.5	0.2	0.30	7.58	5.56
8	Ghansiali-T	A	42	0.12	0.08	1.47	0.18	0.26	7.58	7.02
9	Karnprayag-L	A	73	0.06	0.04	1.69	0.34	0.34	3.2	2.9
10	Karnprayag-T	A	73	0.08	0.04	2.11	0.34	0.33	2.3	2.5
11	Kosani-L	A	152	0.03	0.02	1.54	0.2	0.25	1.9	2.11
12	Kosani-T	A	152	0.03	0.02	2.07	0.18	0.24	1.1	1.54
13	Koteshwar-L	A	64	0.10	0.05	1.95	0.24	0.30	5.4	5.65
14	Koteshwar-T	A	64	0.07	0.04	1.69	0.28	0.33	4.2	4.1
15	Koti-L	A	98	0.04	0.03	1.46	0.34	0.54	2.6	2.52
16	Koti- T	A	98	0.02	0.02	0.90	0.36	0.45	2.5	2.59
17	Purola-L	A	67	0.08	0.05	1.57	0.2	0.29	3.2	4.06
18	Purola-T	A	67	0.09	0.05	2.04	0.2	0.29	5.6	5.87
19	Rudraprayag-L	A	60	0.05	0.02	2.58	0.12	0.15	2.6	2.25
20	Rudraprayag-T	A	60	0.05	0.03	1.91	0.12	0.17	2.2	2.15
21	Srinagar-L	A	62	0.07	0.02	3.44	0.08	0.16	2	3.15
22	Srinagar-T	A	62	0.05	0.02	2.50	0.08	0.19	3.2	3.29
23	Tehri-L	A	53	0.07	0.04	1.73	0.32	0.42	4.7	4.5

(Continued)

Table6. (Continued)

S. No.	EQ record	Soil Type	Dist. (km)	PGA (g)	PGV (m/s)	A/V (g/m/s)	Frequency Parameter		Drift Wall 1 U (mm)	Drift Wall 2 U (mm)
							T_p	T_m		
24	Tehri-T	A	53	0.06	0.09	0.68	0.26	0.71	7.58	11.45
25	Uttarakashi-L	A	31	0.24	0.17	1.42	0.24	0.29	7.58	15.84
26	Uttarakashi-T	A	31	0.31	0.20	1.59	0.24	0.29	7.58	16

As the natural period of the URM walls lies in the acceleration sensitive region of the response spectra of most grounds motions (except for the Sikkim earthquake), the PGA is selected to represent the ground motion intensity. The displacement of the URM walls is plotted against PGA values of individual ground motions in Figures 5 and 6. The limit states of cracking, strength, and collapse obtained from the backbone curve are plotted in the figures for reference. For the wall with the smaller axial load and time period 0.1s, ground motions with PGA below 0.02g result in displacements less than 0.5 mm and cause little cracking or no damage. Ground motions with PGA values between 0.02 and 0.05g cause the URM wall to reach displacement limit corresponding to the wall's shear strength. A linearly increasing trend is observed between the PGA and the observed displacement up to a PGA value of 0.1g. Ground motions with PGA values above 0.1g lead to high displacements (over 7.6mm) and cause the collapse of the URM wall. In the case of the wall with higher axial stress and time period 0.3s, ground motions with PGA below 0.04g, result in displacements less than 1 mm and cause little cracking or no damage to the URM wall. Ground motions with PGA values between 0.08 and 0.14g cause the wall to reach its shear strength. The PGA exhibits a linearly increasing relationship with the observed displacement, till a PGA value of 0.14g. Ground motions with PGA values above 0.14g lead to high displacements (over 16mm) and cause collapse. The URM wall with a higher imposed load resists seismic waves with slightly higher PGA before the collapse.

While the general trends indicate an overall linear relationship between displacement and PGA, it is also observed that in a few cases the response of the URM walls differs from these trends (shown marked in Figures 5 and 6). In a few cases, the strength limit state is observed at low PGA while at a

Figure 5. Wall (lower axial load): drift versus peak ground acceleration.
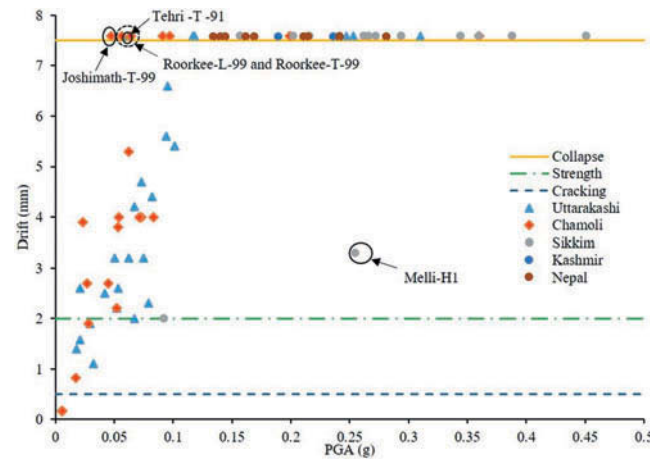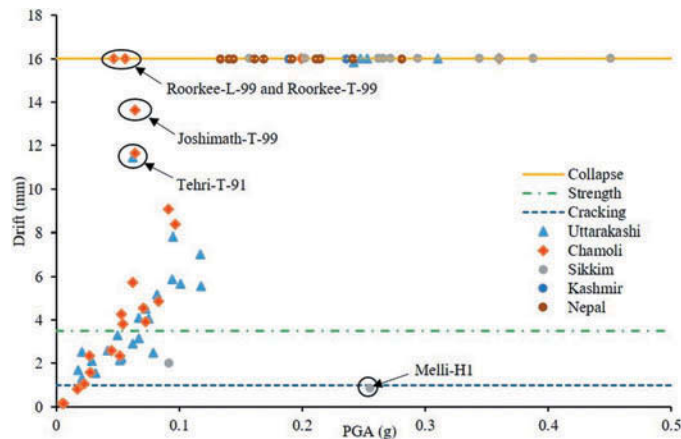

Figure 6. Wall (higher axial load): drift versus peak ground acceleration.

large PGA (greater than 0.2g), very low displacements are recorded. The ground motions corresponding to the cases which exceeded the strength limit state at low PGA are shown in Figures 7 and 8. The presence of sharp velocity pulses in the low PGA seismic records, Joshimath-T (from the 1999 Chamoli database) and Tehri-T (from the 1991 Uttarkashi database) caused the URM Walls to collapse. In both cases, observations of the time history output of the URM walls indicate that immediately after the arrival of the velocity pulse, the walls experienced high strength demand. This is followed by strength and stiffness degradation, causing the URM walls to exhibit high displacements. In particular, the URM wall with lower axial load reached its collapse displacement limit of 7.5mm under both pulse ground motions. While the URM wall with higher axial stress did not collapse under these two pulse motions, it experienced displacements which were close to its collapse displacement limit.

The response spectra of the two records with pulse characteristics also exhibit wide bi-modal characteristics (shown in Figure 9). Hysteresis loops from the quasi-static experimental tests indicate that the stiffness of the URM wall with low axial stress, decreased nine-fold during the tests, and hence the natural time period of the wall exhibits a three-fold increase during severe ground motions, making it susceptible to damage under wide/bi-modal spectra. Under the two

Figure 7. Velocity pulse in the Joshimath-T record from the 1999 Chamoli earthquake.
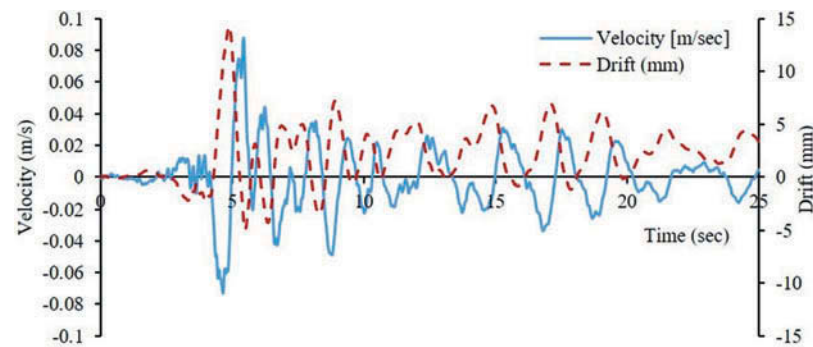
Figure 8. Velocity pulse in the Tehri-T record from the 1991 Uttarkashi earthquake.
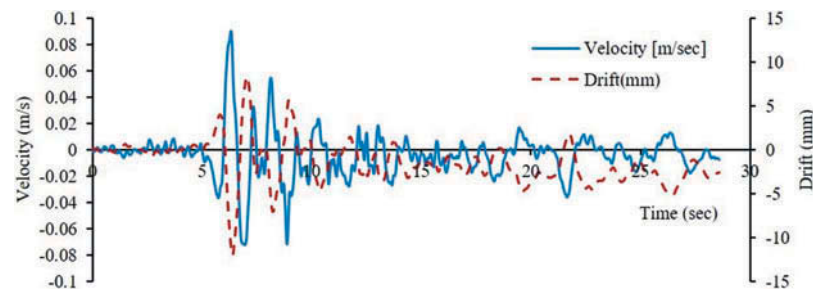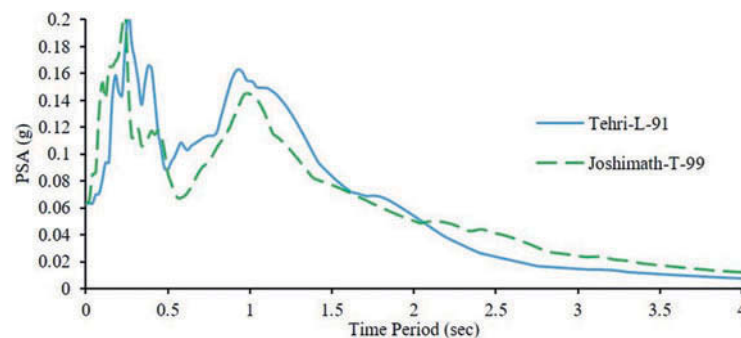

**Figure 9. Wide/Bi modal response spectra (1999 Chamoli earthquake).**

ground motions, the stiffness of this URM wall was observed to decrease six-fold and nine-fold, respectively. Similarly, the experimental test response of the URM wall with high axial stress exhibits a decrease in stiffness by a factor of three. The low PGA levels of both records indicate that the high displacement of these walls was due to the combined effect of velocity pulses along with the wide acceleration sensitive response spectra. Ground motions with "pulse" velocity features and *wide/bi-modal* response spectra have been reported to cause higher damage to a structure. Pulse-type motions exhibiting *wide* acceleration sensitive region in the response spectra result in higher strength demand (Chopra & Chintanapakdee, 2001; Malhotra, 1999) and also imposes a large displacement demand (Kalkan & Kunnath, 2006).

Two ground motions from the 1999 Chamoli earthquake, recorded at the Roorkee station (soil type C; equivalent to soil type D/E as per ASCE 7–10 (American Society of Civil Engineers, 2010) exhibited peculiar response spectra as shown in Figure 10a. An increasing trend is exhibited, till a weak peak is observed at 0.8s followed by a sharp peak at 1.5s. As seen from Table4 ,both URM walls analyzed in this study exhibited high displacements and collapsed under these two weak ground motions. On the contrary, a high PGA ground motion, *Melli-H1*, from the 2011 Sikkim earthquake resulted in low values of storey displacement. The reduced displacements are possibly due to the extremely high-frequency content in this ground motion, as seen in Figure 10b, which may not have allowed the URM Walls enough time to respond in any particular direction.

Observations of displacements from Tables 2 to 6 indicate that NTHA performed using ground motions from the 2005 Kashmir earthquake, the 2015 Nepal earthquake and the 2011 Sikkim earthquake resulted in high displacements corresponding to complete damage of URM walls. Post-earthquake field reports obtained from the literature for these three earthquakes indicate heavy damage to URM structures. Extensive damage to masonry structures in the Sikkim earthquake, in particular to buildings in the towns of Gangtok, Chungthang, Mangan and Singtam has been reported (Rajendran et al., 2011). In the present study, collapse of walls is predicted by NTHA, using ground motions corresponding to these towns. The 2005 Kashmir earthquake caused widespread damage to URM structures, and the post-earthquake reconnaissance studies classified the performance of URM structures as "collapse prevention or worse" (Rossetto & Peiris, 2009). In this study, both records from Abbottabad used for NTHA resulted in high displacements leading to complete collapse of both URM walls. Similarly, traditional URM structures performed poorly in the Nepal earthquake (Whitney & Agrawal, 2017). All ten records from Nepal earthquake used for NTHA in the current study caused high displacements leading to collapse, corresponding well with the damage reported from the post-earthquake survey.

However, post-earthquake field reports from the 1991 Uttarakashi earthquake and the 1999 Chamoli earthquake report a wide variation in observed damages. In the 1991 Uttarkashi

Figure 10. (a) Response spectra for Roorkee (1999 Chamoli) and (b) FFT of Melli-H1 (2011 Sikkim).
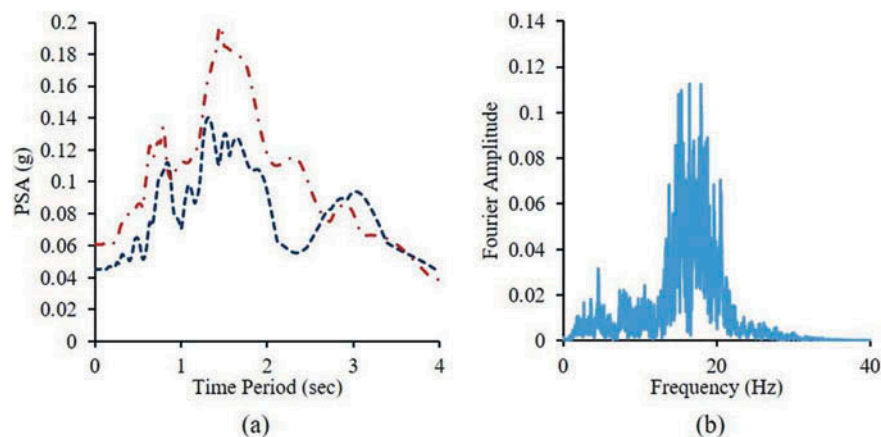
earthquake, MMI Intensity VIII was assigned to the epicentral area thus classifying the damage as "severe." MMI level VIII corresponds to "great damage in poorly built structures, fall of monuments, walls, chimneys, etc." The buildings in the towns of Uttarkashi and Bhatwari suffered severe cracking and collapse (Arya, 1992). In the present study, ground motions from these two towns used for NTHA corresponded to high displacements leading to collapse of URM walls. In towns further from the epicenter, the assigned MMI intensity levels ranged from VI to IV. A corresponding variation in displacements is accordingly observed in the present study. Shrikhande

Rai, Narayan, and Das (2000) and Jain et al. (1999) discuss the performance of structures in the Chamoli earthquake. There was extensive damage to the twin cities of Chamoli and Gopeshwar and the neighboring district of Rudraprayag and an MSK intensity level of VIII, corresponding to "considerable damage" was assigned to a few locations. Shaking under such an intensity level causes older structures sustain considerable damage and partially collapse. Shrikhande et al. (2000) report that most of the houses in the epicentral area "were razed to the ground or were partially collapsed." In-plane shear failure of brick masonry walls was also reported. In the present study, ground motions from Gopeshwar and Ukhimath town used for NTHA showed high displacements corresponding to collapse of URM walls. In towns further from the epicenter, MMI intensity level of VI corresponding to visible damage to masonry structures was assigned. A corresponding variation in displacements is accordingly observed in the present study.

Further, in the 1999 Chamoli quake, the influence of local geology and topography was mainly observed in the frequency content of recorded accelerograms (Shrikhande et al., 2000). As seen in Figure 11, ground motions recorded at Gopeshwar, situated near the valley, have lower ranges of frequency content for the near-field motions (Shrikhande et al., 2000). Ground motions recorded at Ukhimath station, which is situated on a hilltop, have higher ranges of frequency content.

Ground motions with frequency parameters close to the natural frequency of the structure may cause increased values of displacement. In this study, a weak correlation is observed between wall displacements and frequency parameters of the Chamoli earthquake, which results in a slight increase in displacement values. However, for the other earthquakes, a weak correlation is observed between wall displacements and frequency parameters. The correlation coefficients are tabulated in Table 7. It is observed that the frequency content of the earthquake is a secondary parameter which may explain damage only in some instances.

5. Summary

Observations of tabulated displacements indicate that NTHA performed using ground motions from the 2005 Kashmir earthquake, the 2015 Nepal earthquake and the 2011 Sikkim earthquake resulted in high displacements corresponding to complete damage of low strength URM walls. These analytical results compare favourably with the post-earthquake field studies from these

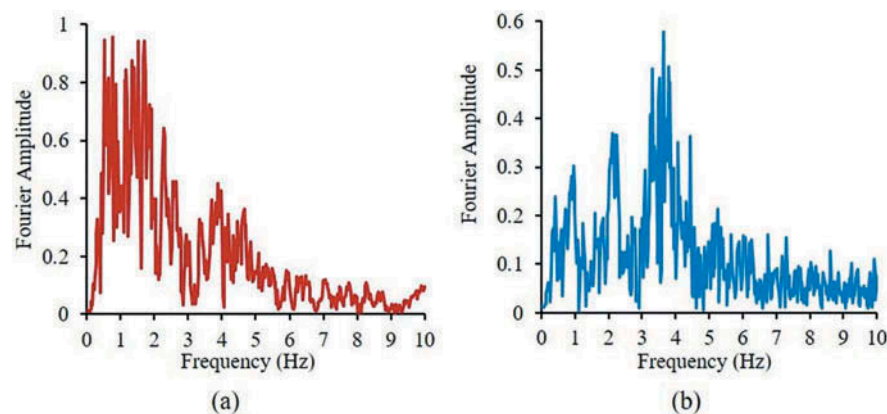**Figure 11. (a)FFT of Gopeshwar—L record and (b) Ukhimath—T record (1999 Chamoli).**

cogent ·· engineering

Table 7. Correlation coefficients for drift versus ground motion frequency content				
Earthquake	Wall 1		Wall 2	
	T_p (s)	T_m (s)	T_p (s)	T_m (s)
1991 Uttarkashi	0.03	0.003	0.13	0.003
1999 Chamoli	0.35	0.46	0.43	0.67
2011 Sikkim	0.03	0.05	0.04	0.07
2015 Nepal	0	0	0	0
2005 Kashmir	0	0	0	0

three earthquakes which report significant to catastrophic damage to masonry structures. NTHA performed using ground motions from the 1991 Uttarkashi earthquake, and the 1999 Chamoli earthquake present a variation in displacements, ranging from *no damage* to *collapse*. The results compare favorably with reconnaissance studies carried out in the aftermath of the two earthquakes where varying levels of damage intensity were assigned to different regions, based on the wide variation in observed damage.

While grounds motions with low PGA values caused low displacements, ground motions with moderate PGA values caused the URM walls to reach their strength and exhibit moderate hysteresis loops. Diagonal cracking in shear walls occurs close to the peak shear force. Ground motions with high PGA levels excited the walls to the post-peak regime causing collapse. The post-peak response of shear walls is characterized by rapid strength and stiffness degradation and also higher energy dissipation.

Stiff URM structures, having low natural time period are vulnerable under moderate to high PGA seismic waves. It is known that dynamic response of structures is also sensitive to the frequency content of the ground motion. However, in the present study, it is observed that there is a very weak correlation between the displacements and frequency parameters. It may be inferred that the frequency content of the earthquake is a secondary parameter which may explain damage only in some instances. URM shear walls exhibit rapid stiffness degradation and their fundamental period elongates during the duration of the strong motion, thus increasing their vulnerability to ground motions with wide response spectra. Pulse ground motions were notably observed to have a damaging effect on low strength URM walls.

6. Conclusions

The behavior of both low strength shear walls examined in this study was found to be brittle in nature. Low strength URM shear walls with a lower level of pre-compression are more vulnerable than walls with high levels of pre-compression. Wall 1 ($p = 0.6$MPa) and wall 2 ($p = 1.24$ MPa) collapse under PGA levels of 0.1g and 0.14g, respectively. As the Himalayan region lies in the high seismic zone, ground motions with PGA levels greater than 0.1g are expected. Low strength URM shear walls would collapse or be heavily damaged under such expected ground motions. Accordingly, URM walls in this region must be retrofitted to resist the high displacements corresponding to the PGA levels.

However, due to differences in the material properties, the previous research work on URM structures cannot be compared directly with the present work on URM shear walls. The conclusions from this study are limited to walls having aspect ratio and axial stress similar to the two shear walls considered for investigation. The effect of axial stress, material properties and boundary conditions on the seismic behavior of masonry walls, can be further investigated. The findings of this study may be generalized by considering different types of URM walls prevalent in the Himalayan region.

cogent ··engineering

Author details
Jayaprakash Vemuri[1]
E-mail: ce13p1006@iith.ac.in
ORCID ID: http://orcid.org/0000-0002-9480-790X
Syed Ehteshamuddin[1]
E-mail: ce15mtech11025@iith.ac.in
Subramaniam V. L. Kolluru[1]
E-mail: kvls@iith.ac.in
[1] Department of Civil Engineering, IIT Hyderabad, Sangareddy, India.

Citation information
Cite this article as: Evaluation of seismic displacement demand for unreinforced masonry shear walls, Jayaprakash Vemuri, Syed Ehteshamuddin & Subramaniam V. L. Kolluru, *Cogent Engineering* (2018), 5: 1480189.

References
Abrams, D. P. (1992, July). Strength and behavior of unreinforced masonry elements. *Proceedings of the Tenth World Conference on Earthquake* (pp. 19–24). Rotterdam, Balkema.

Ahmad, N., & Ali, Q. (2017). Displacement-based seismic assessment of masonry buildings for global and local failure mechanisms. *Cogent Engineering*, 4(1), 1–33. Taylor & Francis - Online. doi:10.1080/23311916.2017.1414576

Ahmad, N., Ali, Q., Ashraf, M., Alam, B., & Naeem, A. (2012). Seismic vulnerability of the himalayan half-dressed rubble stone masonry structures, experimental and analytical studies. *Natural Hazards and Earth System Sciences*, 12(11), 3441–3454. doi:10.5194/nhess-12-3441-2012

Ahmad, N., Ali, Q., Crowley, H., & Pinho, R. (2014). Earthquake loss estimation of residential buildings in Pakistan. *Natural Hazards*, 73(3), 1889–1955. doi:10.1007/s11069-014-1174-8

Ahmad, N., Crowley, H., Pinho, R., & Ali, Q. (2010a). Displacement-based earthquake loss assessment of masonry buildings in Mansehra city, Pakistan. *Journal of Earthquake Engineering*, 14(S1), 1–37. doi:10.1080/13632461003651794

Ahmad, N., Crowley, H., Pinho, R., & Ali, Q. (2010b). Simplified formulae for the displacement capacity, energy dissipation, and characteristic vibration period of brick masonry buildings. 8IMC-Dresden Germany. *Proceedings of the International Masonry Society*, 11(2–H), 1385–1394.

Ahmad, N., Crowley, H., Pinho, R., Ali, Q., & Aziz, S. (2011). Development of Fast Building Seismic Screening (FBSS) Method. International Conference on Earthquake Engineering and Seismology, NUST, Islamabad, Pakistan.

Ali, Q., Badrashi, Y. I., Ahmad, N., Alam, B., Rehman, S., & Banori, F. A. S. (2012). Experimental investigation on the characterization of solid clay brick masonry for lateral shear strength evaluation. *International Journal of Earth Sciences and Engineering*, 05(04), 782–791.

Ali, Q., Naeem, A., Ashraf, M., Ahmed, A., Alam, B., Ahmad, N., . . . Umar, M. (2013). Seismic performance of stone masonry buildings used in the Himalayan Belt. *Earthquake Spectra*, 29(04), 1159–1181. doi:10.1193/091711EQS228M

Alsuwwi, A. H., Hassan, M., Awwad, J., & Ahmad, N. (2015). Comparative analysis of cement-sand & cement-sand-khaka (stone dust) mortar shear wall brick masonry materials. *Masonry International*, 28(01), 1–10.

American Society of Civil Engineers. (2010). *Minimum design loads for buildings and other structures*. Reston, VA: ASCE/SEI Standard 7-10. Virginia: ASCE.

Anthoine, A., Magonette, G., & Magenes, G. (1995). Shear compression testing and analysis of brick masonry walls. *Proceedings of the Tenth European Conference on Earthquake Engineering*. 28 Aug- 2 Sep. Balkema, Rotterdam.

Arya, A.S. (1992) October 20, 1991. Uttarkashi (India) earthquake, Tenth World Conference on Earthquake Engineering, 19-24 July, Balkema, Rotterdam, 7039-7044.

Bilham, R., & Wallace, K. (2005). Future Mw 8 earthquakes in the Himalaya: Implications from the 26 Dec 2004 Mw 9.0 earthquake on India's eastern plate margin. *Special Publication of Geological Survey of India, 85*, 1–14.

Bosiljkov, V., Page, A. W., Bokan-Bosiljkov, V., & Zarnik, R. (2010). Evaluation of the seismic performance of brick masonry walls. *Structural Control and Health Monitoring, 17*(1), 100–118. doi:10.1002/stc.v17:1

Bothara, J. K., & Hicyilmaz, K. M. O. (2008). General observations of building behaviour during the 8th October 2005 Pakistan earthquake. *Bulletin of the New Zealand Society for Earthquake Engineering, 41*(4), 209–233.

Boussabah, L., & Bruneau, M. (1992). Review of the seismic performance of unreinforced masonry walls. *Proceedings of the Tenth World Conference on Earthquake Engineering*. 19-24 July, (pp. 4537–4540). Rotterdam. Balkema.

Bureau of Indian Standards. (1991). *Handbook on masonry design and construction, SP:20*. New Delhi: BIS.

Bureau of Indian Standards. (2002). *IS: 1893 Indian standard criteria for earthquake resistant design of structures: Part 1– General provisions and buildings*. New Delhi: BIS.

Chopra, A. K. (2012). *Dynamics of structures: Theory and applications to earthquake engineering*. New Jersey, NJ: Pearson Prentice Hall.

Chopra, A. K., & Chintanapakdee, C. (2001). Comparing response of SDF systems to near-fault and far-fault earthquake motions in the context of spectral regions. *Earthquake Engineering and Structural Dynamics, 30*(12), 1769–1789. doi:10.1002/eqe.92

Computers and Structures Incorporated. (2012). *SAP2000 version 15, software*. Berkeley, CA.

Consortium of Organizations for Strong-Motion Observation Systems. (2015). *Earthquake data web page for India, California, USA*. Retrieved from http://www.strongmotioncenter.org/vdc/scripts/earthquakes.plx#IND

Durrani, A. J., Elnashai, A. S., Hashash, Y. M. A., Kim, S. J., & Masud, A. (2005). *The Kashmir earthquake of October 08, 2005: A quick look report*. USA: Mid-America Earthquake Center, University of Illinois at Urbana-Champaign.

Elenas, A, & Meskouris, K. (2001). Correlation study between seismic acceleration parameters and damage indices of structures. *Engineering Structures, 23*(6), 698-704. doi: 10.1016/S0141-0296(00)00074-2

FEMA 307. (1999). Evaluation of earthquake damaged concrete and masonry wall buildings - technical resources. Washington, D.C: Federal Emergency Management Agency.

Formisano, A. (2012). Seismic damage assessment of school buildings after 2012 Emilia Romagna earthquake. *Ingegneria Sismica, 29*(2–3), 72–86.

Formisano, A., Florio, G., Landolfo, R., & Mazzolani, F. M. (2011). Numerical calibration of a simplified procedure for the seismic behaviour assessment of masonry building aggregates. *Proceedings of the 13th International Conference on Civil, Structural and Environmental Engineering Computing*, p. 28, Stirlingshire, Scotland. doi:10.4203/ccp.96.172

Formisano, A., & Marzo, A. (2017). Simplified and refined methods for seismic vulnerability assessment and retrofitting of an Italian cultural heritage masonry building. *Computers and Structures, 180*, 13–26. doi:10.1016/j.compstruc.2016.07.005

Jain, S. K., Murty, C. V. R., Arlekar, J. N., Rajendran, C. P., Rajendran, K., & Sinha, R. (1999). Chamoli (Himalaya, India) Earthquake of 29 March 1999", EERI special earthquake report. *EERI Newsletter, 33*(7), 8.

Javed, M., Naeem, A., & Magenes, G. (2008). Performance of masonry structures during earthquake-2005 in Kashmir. *Mehran University Research Journal of Engineering Technology, 27*(3), 271–282.

Joshi, A. (2006). Analysis of strong motion data of the Uttarkashi Earthquake of 20th October 1991 and the Chamoli earthquake of 28th March 1999 for determining the Q value and source parameters. *ISET Journal of Earthquake Technology, 43*(1–2), 11–29.

Kalkan, E., & Kunnath, S. K. (2006). Effects of fling step and forward directivity on seismic response of buildings. *Earthquake Spectra, 22*(2), 367–390. doi:10.1193/1.2192560

Kayal, J. R. (2001). Microearthquake activity in some parts of the Himalaya and the tectonic model. *Tectonophysics, 339*(3–4), 331–351. doi:10.1016/S0040-1951(01)00129-9

Khan, S., Khan, A. N., Elnashai, A. S., Ashraf, M., Javed, M., Naseer, A., & Alam, B. (2013). Experimental seismic evaluation of unreinforced brick masonry buildings. *Earthquake Spectra, 28*(3), 1269–1290.

Magenes, G., & Calvi, G. M. (1992). Cyclic behaviour of brick masonry walls. *Proceedings of the Tenth World Conference on Earthquake Engineering.* 19-24 July, (pp. 3517–3522). Balkema, Rotterdam.

Magenes, G., & Calvi, M. (1997). In-plane seismic response of brick masonry walls. *Earthquake Engineering & Structural Dynamics, 26*(11), 1091–1112. doi:10.1002/(ISSN)1096-9845

Malhotra, P. K. (1999). Response of buildings to near-field pulse-like ground motions. *Earthquake Engineering & Structural Dynamics, 28*, 1309–1326. doi:10.1002/(ISSN)1096-9845

Mandal, P., Chadha, R. K., Kumar, N., Raju, I. P., & Satyamurty, C. (2007). Source parameters of the deadly M_w 7.6 Kashmir earthquake of 8 October 2005. *Pure and Applied Geophysics, 164*(10), 1963–1983. doi:10.1007/s00024-007-0258-8

Mandal, P., Rastogi, B. K., & Gupta, H. K. (2000). Recent Indian earthquakes. *Current Science, 79*(9), 1334–1346.

Mann, W., & Muller, H. (1982). Failure of shear stressed masonry. An enlarged theory, tests and application to shear walls. *Proceedings of the British Ceramic Society, 30*, 223–235.

Mittal, H., Kumar, A., & Ramhmachhuani, R. (2012). Indian national strong motion instrumentation network and site characterization of its stations. *International Journal of Geosciences, 3*(6A), 1151–1167. doi:10.4236/ijg.2012.326117

Moon, L., Dizhur, D., Senaldi, I., Derakhshan, H., Griffith, M., Magenes, G., & Ingham, J. (2014). The demise of the URM building stock in Christchurch during the 2010-2011 Canterbury earthquake sequence. *Earthquake Spectra, 30*(1), 253–276. doi:10.1193/022113EQS044M

Moore, T. A., Kobzeff, J. H., Diri, J., & Arnold, C. (1988). The Whittier narrows, California earthquake of October 1, 1987 – Preliminary evaluation of the performance of strengthened unreinforced masonry buildings. *Earthquake Spectra, 4*(1), 197–212. doi:10.1193/1.1585472

Naseer, A., Naeem, A., Hussain, Z., & Ali, Q. (2010). Observed seismic behavior of buildings in northern Pakistan during the 2005 Kashmir earthquake. *Earthquake Spectra, 26*(2), 425–449. doi:10.1193/1.3383119

Ni, J., & Barazangi, M. (1984). Seismotectonics of the Himalayan collision zone: Geometry of the underthrusting Indian plate beneath the Himalayas. *Journal of Geophysical Research: Solid Earth, 89*(B2), 1147–1163. doi:10.1029/JB089iB02p01147

Parameswaran, R. M., Natarajan, T., Rajendran, K., Rajendran, C. P., Mallick, R., Wood, M., & Lekhak, H. C. (2015). *Journal of Asian Earth Sciences, 111*, 161-174.

Penelis, G. R. G. (2006). An efficient approach for pushover analysis of Unreinforced Masonry (URM) structures. *Journal of Earthquake Engineering, 10*(3), 359–379. doi:10.1080/13632460609350601

Program for Excellence in Strong Motion Studies. (201532). *Earthquake data web page, Roorkee, India.* Retrieved from http://www.pesmos.in

Rai, D. C., Singhal, V., Mondal, G., Parool, N., Pradhan, T., & Mitra, K. (2012). The M 6.9 Sikkim (India–Nepal Border) earthquake of 18 September 2011. *Current Science, 102*(10), 1437–1446.

Rajendran, K., Rajendra, C. P., Thulasiraman, N., Andrews, R., & Sherpa, N. (2011). The 18 September 2011, North Sikkim earthquake. *Current Science, 101*(11), 1475–1479.

Reitherman, R. (1985). The Borah Peak, Idaho earthquake of October 28, 1983 – Performance of unreinforced masonry buildings in Mackay, Idaho. *Earthquake Spectra, 2*(1), 205–224. doi:10.1193/1.1585309

Rossetto, T., & Peiris, N. (2009). Observations of damage due to the Kashmir Earthquake of October 8, 2005 and study of current seismic provisions for buildings in Pakistan. *Bulletin of Earthquake Engineering, 7*(3), 681–699. doi:10.1007/s10518-009-9118-5

Seeber, L., & Armbruster, J. G. (1981). Great detachment earthquakes along the Himalayan arc and long term forecasting. In *Earthquake prediction—An international review*, Maurice Ewing Series (pp. 259–277). Washington, DC: American Geophysical Union. http://dx.doi.org/10.1029/me004p0259

Shrikhande, M., Rai, D. C., Narayan, J., & Das, J. (2000). The March 29 earthquake at Chamoli, India. *Proceedings of the Twelfth World Conference on Earthquake Engineering*, Auckland, New Zealand.

Sinvhal, A. (2010). *Understanding earthquake disasters* (1st ed.). India: Tata Mc-Graw Hill Education Private Limited.

Somers, P., Campi, D., Holmes, W., Kehoe, B. E., Klingner, R. E., Lizundia, B., & Schmid, B. (1996). Unreinforced masonry buildings. *Earthquake Spectra, 12*(S1), 195–217. doi:10.1193/1.1585926

Whitney, R., & Agrawal, A. K. (2017). Ground motion characteristics of the 2015 Gorkha, Nepal, earthquake and its effects on a prototype unreinforced masonry building. *Journal of Structural Engineering,* 143(4), 1–10. doi:10.1061/(ASCE)ST.1943-541X.0001717

World Housing Encyclopaedia – Prompt Assessment of Global Earthquakes for Response (WHE-PAGER) Survey. (2007). CA. Retrieved from http://www.world-housing.net/related-projects/whe-pager-project/about-this-project

Cogent Engineering (ISSN: 2331-1916) is published by Cogent OA, part of Taylor & Francis Group.

Publishing with Cogent OA ensures:

- Immediate, universal access to your article on publication
- High visibility and discoverability via the Cogent OA website as well as Taylor & Francis Online
- Download and citation statistics for your article
- Rapid online publication
- Input from, and dialog with, expert editors and editorial boards
- Retention of full copyright of your article
- Guaranteed legacy preservation of your article
- Discounts and waivers for authors in developing regions

Submit your manuscript to a Cogent OA journal at www.CogentOA.com